Lab on a Chip

RSC Publishing

PAPER

View Article Online
View Journal | View Issue

Cite this: *Lab Chip*, 2013, **13**, 1762

Rapid patterning of 'tunable' hydrophobic valves on disposable microchips by laser printer lithography†

Yiwen Ouyang,[a] Shibo Wang,[b] Jingyi Li,[a] Paul S. Riehl,[a] Matthew Begley[c] and James P. Landers*[ade]

Received 19th November 2012,
Accepted 11th February 2013

DOI: 10.1039/c3lc41275j

www.rsc.org/loc

We recently defined a method for fabricating multilayer microdevices using poly(ethylene terephthalate) transparency film and printer toner, and showed these could be successfully applied to DNA extraction and amplification (Duarte *et al.*, *Anal. Chem*. 2011, **83**, 5182–5189). Here, we advance the functionality of these microdevices with flow control enabled by hydrophobic valves patterned using laser printer lithography. Laser printer patterning of toner within the microchannel induces a dramatic change in surface hydrophobicity (change in contact angle of DI water from 51° to 111°) with good reproducibility. Moreover, the hydrophobicity of the surface can be controlled by altering the density of the patterned toner *via* varying the gray-scale setting on the laser printer, which consequently tunes the valve's burst pressure. Toner density provided a larger burst pressure bandwidth (158 ± 18 Pa to 573 ± 16 Pa) than could be achieved by varying channel geometry (492 ± 18 Pa to 573 ± 16 Pa). Finally, we used a series of tuned toner valves (with varied gray-scale) for passive valve-based fluidic transfer in a predictable manner through the architecture of a rotating PeT microdevice. While an elementary demonstration, this presents the possibility for simplistic and cost-effective microdevices with valved fluid flow control to be fabricated using nothing more than a laser printer, a laser cutter and a laminator.

Introduction

Since the inception of microfluidics the 1980's, we have seen lab-on-chip (LOC) technologies increasingly applied to a broad variety of applications including immunoassays,[1–3] enzyme assays,[4–6] the polymerase chain reaction (PCR),[7,8] DNA analysis,[9,10] protein separation,[11,12] cell analysis.[13,14] The 1990's saw order of magnitude reduction in analysis time (*e.g.*, electrophoretic separation), volume of reagents consumed and volume of sample required for analysis in microfluidic devices. However, it became clear that expediting the ''analytical step'' provided only incremental improvement to the overall analysis time when sequential sample preparation steps were involved. Hence, integration of sample preparation was critical, and the ability to do so requires that very different chemistries be physically-isolated in the microfluidic architecture of the device, but ultimately connectable when needed.[15,16] This brought to the forefront need for a 'valving' solution in the microfluidic regime.

It has become almost commonplace to see microfluidic systems described in the literature with a variety of microvalving approaches that serve as a core component for a comprehensive flow control.[17–20] Disposable microdevices with such valves are particularly practical when used for handling biohazardous materials as it provides a 'closed' system. However, the availability of commercially-available LOC technologies has been partially limited by the ability to manufacture disposable microdevice with reliable microvalves at an economically-viable cost. Desirable features of a disposable microdevice with integrated microvalves include those: (1) fabricated with substrate that is cost-effective, (2) compatible with current industrial microdevice manufacturing techniques, (3) easily integrated in the manufacturing process, and (4) not reliant on external hardware but preferably, use of passive valving mechanisms.

As microfluidics research and development has matured, there has been a shift from traditional glass microdevices to those constructed from polymeric materials, primarily because of ease of fabrication and a decrease in overall cost.[21,22] With the introduction of soft-lithography by Duffy *et al.*, PDMS has become one of the most popular polymeric substrate in

[a]*Department of Chemistry, McCormick Road, University of Virginia, Charlottesville, VA 22904 E-mail: jpl5e@virginia.edu; Fax: (434) 243-8852; Tel: (434) 243-8658*
[b]*Department of Civil and Environmental Engineering, McCormick Road, University of Virginia, Charlottesville, VA 22904*
[c]*College of Engineering, University of California, 3361B Engineering II, Santa Barbara, CA 93105*
[d]*Department of Pathology, University of Virginia Health Science Center, Charlottesville, VA 22908*
[e]*Department of Mechanical Engineering, University of Virginia, Engineer's Way, Charlottesville, VA 22904*

† Electronic supplementary information (ESI) available: Material cost of the PeT microchip; contact angle of DI water on the side wall and photographs showing the surface of the side walls which were laser etched with different ablation parameters. See DOI: 10.1039/c3lc41275j

academia, owing to the large number of devices that can be rapidly replicated from a master template without the need of expensive clean room facilities.[23] Moreover, a series of mechanical valves and geometrically capillary valves have been realized by utilizing the natural elastomeric[24,25] and hydrophobic property[26] of PDMS. Nevertheless, applications of PDMS microdevices to routine biological and chemical purposes has been restricted by its mechanical deformability, instability of the surface treatment, gas permeability and absorption of small hydrophobic molecules.[27]

Thermoplastics provide an alternative to PDMS, and microdevice fabrication with this substrate can benefit from a knowledge base of existing industrial fabrication processes, including multilayer lamination, embossing and injection molding. One of the simplest and least expensive thermoplastic fabrication approaches involves the use of polyester and, in particular, that found in overhead transparency sheets; poly(ethylene terephthalate). do Lago *et al.* were the first to show that black printer toner directly patterned onto the surface of polyester film enables Poly(ethylene terephthalate)-Toner (PeT) microdevices.[28] The toner is bifunctional, serving as the adhesive to bond the two layers together and, where absent, serving to define the fluidic architecture (Fig. 1A). Fabrication of a PeT microdevice was completed by laminating the printed sheet to either a blank transparency film or a sheet with the mirror image of the device design. Under these conditions, the depth of the microchannel was defined by the thickness of the printer toner, which was 7 $\pm$ 1 μm for a single layer of toner (12 $\pm$ 2 μm for two layers). In that work, the PeT microdevice was used for electrophoretic separation of ions with end-channel amperometric detection. This fabrication method was further evolved by Duarte *et al.* to provide deeper channels so that a solid phase could be integrated into the system for DNA extraction.[29] In that work, one or more internal layers of polyester film were laser-ablated and laminated to the toner-patterned layers; again, the toner served as the adhesive but the depth of channel now primarily defined by the number of laser-ablated layers (~100 μm for each internal layer). As a result, they were able to define channels with adequate depth for the extraction and amplification of DNA (>200 μm). PeT microdevices have been successfully utilised for other processes including inducing passive mixing,[30] studying the kinetics of enzymatic reactions,[31] and for rapid protein concentration and purification.[11] In addition, UV laser radiation[32] and chemical surface treatment[33] have made it possible to enhance the protein adsorption on the polyester film surface, as a result, the biofunctionalized polyester film has been applied to ELISA[34] and enzymatic studies.[35]

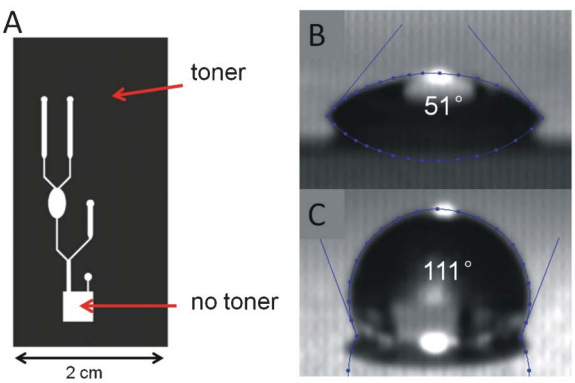

Fig. 1 Controlling the hydrophobicity of the poly(ethylene terephthalate) film. (A) Schematic of an exemplary two-layer PeT microdevice with the microfeatures defined by absence of toner. (B) and (C) Photographic images of deionized water (3 μl) on the surface of unpatterned transparency film and transparency film with a single layer of toner, respectively.

However, it is noteworthy that all of the previous work utilising PeT as a microchip substrate were applied to one-step chemistries (*e.g.*, single reagent delivery). Even though PeT microchips have desirable advantages (ease of fabrication, cost-effectiveness , nonbiofouling for biological samples and desirable optical property used for visual detection[36]), their use has been hindered by the lack of flow control. The reasons for that valving has not been demonstrated on PeT microdevices are the fabrication challenges and the possibility of trading off its inexpensive nature (see ESI†). For example, it is challenging to incorporate into a PeT microdevice the type of mechanically-driven active valves that have been a cornerstone for PDMS microdevices, primarily because the required feature size that would prevent microchip debonding is excessively large (*i.e.*, the fluidic resistance of the valve has to be kept small, because the bonding is relatively weak). Non-mechanical active valves, such as phase-change valves (*i.e.*, hydrogel-based,[37] paraffin-based,[38] dissolvable film coupled with centrifugal-pneumatic valves[39]) are a possibility but can malfunction due to thermal- and pressure-induced failure modes during the final lamination step. Moreover, the incorporation of either type of valve necessitates the embedding of a different barrier material, thus, complicating the fabrication. In addition, with the exception of dissolvable film/centrifugal-pneumatic valves,[34] the actuation of such valves generally requires external energy input, again increasing the complexity of operation and potential portability. In contrast, a geometrical capillary valve can be easily fabricated and only requires sufficient driving force to overcome the surface tension of the liquid where the channel dimensions expand. Its operational 'burst pressure' is determined by the aspect ratio of the channel structures, which, in our case, is limited by the resolution for laser ablation (~100 μm) and bonding process (lamination). This creates potential hurdles for accurate fabrication of geometric capillary-type valves for fluid flow control. As a result, PeT as substrate has not been as widely-utilized for microchip fabrication as other thermoplastics (*e.g.*, PMMA or PC) materials that ultimately are substantially more costly.

In this work, we provide the first valving solution for integrating fluidic control functionality into PeT microdevices, while keeping the fabrication process, that is 'print, cut and laminate', as simple as it was defined by do Lago *et al.*[28] More specifically, hydrophobic valves have been patterned onto the

polyester film by laser printing lithography, and these function as passive valves. In addition to showing how these devices can be fabricated, we discuss the fundamental principles behind using a conventional laser printer to control the degree of hydrophobicity/hydrophilicity of the surface, and the effect of valve surface character on burst pressure. Both our theoretical model and experimental results suggest that the burst pressure of the valve is defined by the density of the toner particles on the film, which is simply controlled by the gray scale in the printing setting. Finally, we demonstrate ability of the toner-based hydrophobic valves to provide advanced control of sequential fluidic manipulation processes driven by centrifugal force. Since this fabrication method is compatible with the current fabrication approaches for creating PeT microdevices, it presents an interesting potential for developing PeT microchips as low-cost microfluidic-based diagnostic devices in resource-limited areas.

Theory

Burst pressures associated with printed features

The *Material Safety Data Sheet* (MSDS) for the polyester transparency film used in this work (CG5000, 3M) indicates that the surface coating contains silica, and this is likely responsible for rendering the surface hydrophilic (Fig. 1B). Conversely, the printer toner particles are primarily wax-based[28] and, if patterned on the surface, should increase the hydrophobic character (Fig. 1C). As expected, the degree of hydrophobicity imparted to the transparency film surface by micropatterning with toner is revealed by a change in the contact angle as the composition of the heterogeneous solid surface is altered. In many instances, the effective wetting angle of a patterned surface can be described by a simple rule of mixtures (*i.e.* Cassies equation), as in:

$$\cos\theta_p = f\cos\theta_t + (1 - f)\cos\theta_f \quad (1)$$

In the following, we construct a hydrophobic valve by printing toner patches at various gray scales on the top and bottom of a channel formed by the lamination process, as shown in Fig. 2. Fluid easily flows to the leading edge of the patterned feature due to the hydrophilic nature of the Pe surface (Fig. 3). Additional pressure is needed to drive the fluid front past the leading edge of the patterned section. The pressure change across the meniscus (when located on the toner patch) associated with equilibrium (*i.e.* force balance) is given by:

$$\Delta P = 2\gamma\left(\frac{\cos\theta_w}{w} + \frac{\cos\theta_p}{h}\right) \quad (2)$$

where γ is the surface tension of the liquid, h is the height of the channel, w is the channel width, $\cos\theta_w$ is the contact angle

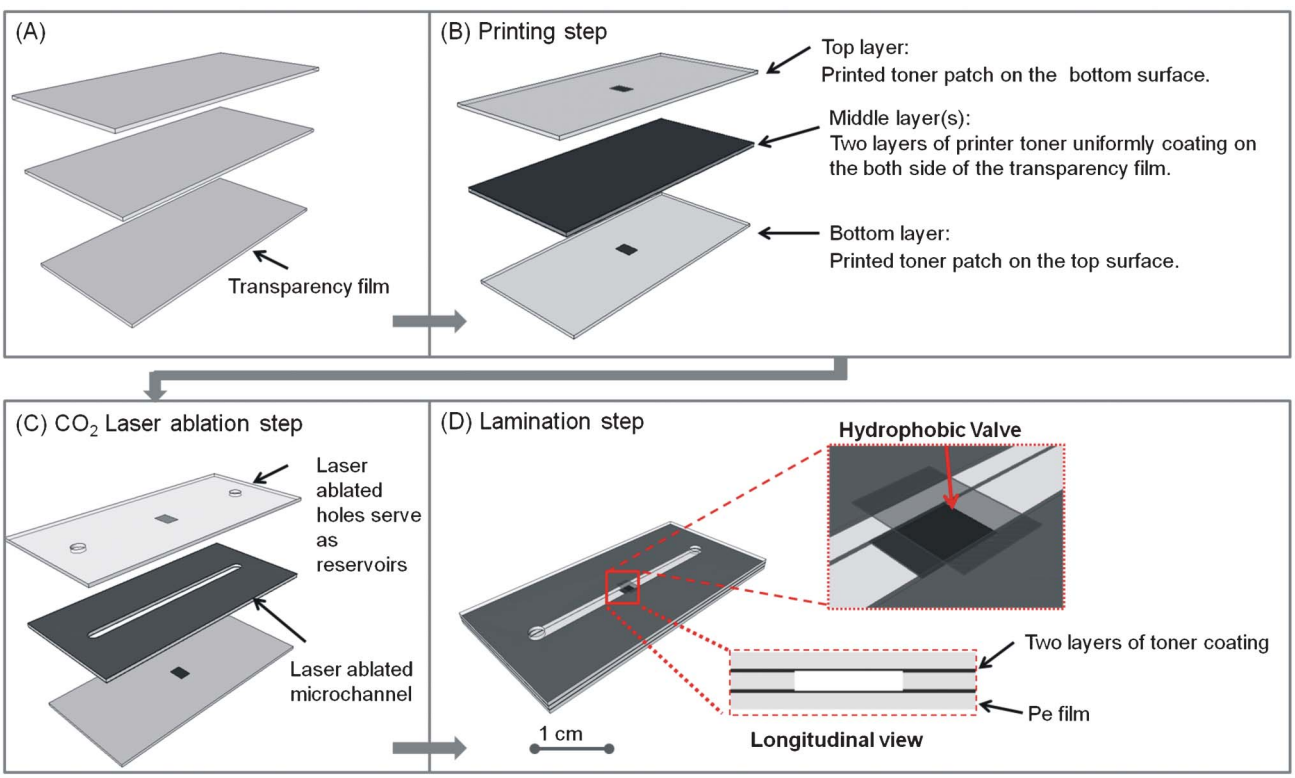

Fig. 2 Steps involved in the fabrication of a PeT microdevice with hydrophobic toner-based valves. (A) Three layers of transparency film, (B) patterning toner onto the both sides of the middle layer and hydrophobic patches on the top and bottom layers, (C) microfeatures cut by laser cutter in to middle layers and, (D) alignment of all layers for lamination.

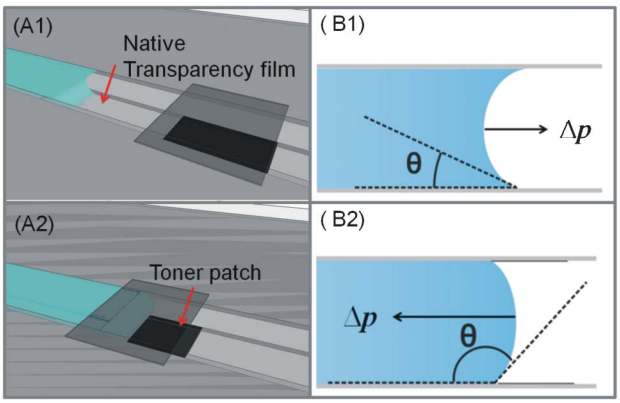

Fig. 3 Configuration and valving mechanism with a toner-based valve. (A) A 3D rendering showing liquid priming the channel with either a hydrophilic ceiling surface (A1) and hydrophobic ceiling surface (A2). (B) A schematic showing wetting interactions with the polyethylene surface without (B1) and with (B2) toner patterning.

of the fluid on the side walls, and again, $\cos\theta_p$ is the contact angle associated with the patterned surface on top and bottom of the channel [given by eqn (1)]. From a theoretical perspective, the apparent dynamic contact angle that exists as the meniscus is advanced by pressure (which is close to the 'critical advancing contact angle') should be used eqn (2).[40] The 'critical advancing contact angle' is the contact angle at which the contact line of liquid/solid begins to move, which is usually greater than the static contact angle (also known as Young-equilibrium contact angle).[41]

Since the sidewall was composed of alternating layers of laser-ablated poly(ethylene terephthalate) and toner strips (Fig. 2D), in principle, the contact angle of the fluid on the side walls could be calculated from the application of rule of mixtures, as done for the patterned surface. However, the laser cutting process significantly alters the surface on the cut edge of the transparency film (which forms the side wall), such that details of the final side-wall geometry following lamination are difficult to quantify. As such, we conducted direct measurements of the pressure needed to stop fluid advancing in the channel without a toner patch, and determined the effective contact angle of the side walls using eqn (2), with $\cos\theta_f$ replacing $\cos\theta_p$ (since there is no patch in these experiments).

It is clear that the burst pressure for the toner-based valves can be tuned by three parameters (1) the physical dimensions of the valve (2) the hydrophobicity of the coating material, and (3) the fractional area of the coating material. Compared with common geometrical capillary valves,[20,21,26] of which the control of the burst pressure relies on no more than two parameters (*i.e.*, the geometry or one invariable hydrophobic property), the use of laser printer lithography technology significantly reduces the dependence on fabrication precision while expanding the operational burst pressure bandwidth. The later is particularly valuable for application to centrifugal systems and is further discussed below.

Burst frequency on a centrifugal system associate with printed features

Considering the radial pressure distribution on the centrifugal system, we use eqn (3) to estimate the pumping pressure generated by centrifugal force:[15]

$$\Delta P = \rho\omega^2(R_2 - R_1)\cdot\left(\frac{R_2 + R_1}{2}\right) = \rho\omega^2\cdot\Delta R\cdot\bar{R} \qquad (3)$$

where ρ is the density of the liquid, ω is the angular velocity of the disc, R_1 and R_2 are the two distances of liquid from the disc center, and ΔR is equal to $R_2 - R_1$ while $\bar{R}$ is equal to $(R_2 + R_1)/2$. Even though it has been successfully applied to predict the burst frequency of other surface tension-based valves,[44,45] it is noteworthy that the pressure calculated from eqn (3) is the equivalent pressure head needed to pump solution in pressure-driven flow at the same flow velocity. Due to the nonuniform centrifugal force density along the radius, the pressure calculated by eqn (3) can deviate slightly from the actual pressure that liquid meniscus experienced at the toner patch.[15]

For the geometry of the channel discussed in this paper, having uniform width and depth, the minimum theoretical pressure to force the liquid of a finite length flowing through this normally 'closed' valve can be calculated by:

$$\Delta P = P_1 - P_2 \qquad (4)$$

where P_1 is the pressure generated on liquid meniscus at the end of the advancing liquid plug on native transparency film and P_2 is the pressure generated on the front meniscus of advancing liquid plug on hydrophobic toner patterned surface, both of which can be calculated by using eqn (2). By combining eqn (2), eqn (3) and eqn (4), the required burst frequency in revolution per minute (rpm) can be calculated by eqn (5).

$$f(\mathrm{RPM}) = \frac{30}{\pi}\sqrt{\frac{2\gamma(\cos\theta_f - \cos\theta_p)}{\rho h\Delta R\bar{R}}} \qquad (5)$$

Material and methods

Reagents

2% (wt/wt) bovine serum albumin (Sigma) was prepared by dissolving in PBS buffer (pH = 7.4, 10 mM). 10 × PCR buffer (Fisher Scientific) was diluted by 10 fold with distilled water. All other reagents are analytical grade and used without further purification. pH of the solution was measured by a Mettler Toledo MP 220 pH meter.

Fabrication of the hydrophobic patches

Commercially available poly(ethylene terephthalate) transparency sheets were used for the base substrate (CG5000, 3M). The thickness of the Pe film was determined to be 110 ± 2 μm thick by a micrometer (IP54, Craftsman) (n = 5). The patterns

for hydrophobic valves were printed on the transparencies using a laser printer with graphic software control. To compare toners from different brands, the setting for the HP laser printer (HP Laserjet 4000) was chosen as '600 dpi' using black toner cartridge (HP C-4127X) and the setting for the Brother printer (Brother HL4070-CDW) was chosen as 'output of RGB for bitmap' and '600 dpi' for four different toner colors (BR-TN-110 Yellow, TN-135 Black, TN-135 Magenta and TN-110 Cyan cartridges). In the evaluation of the efficiency by using gray-scale level control to tuning the hydrophobic surface, only HP laser printer was used to print transparencies with different gray-scale level settings (from 10% to 100% in increments of 10%). After printing, the surface was cleaned by filtered air and did not undergo any further treatment. The thickness of the 100% gray-scale toner patch was measured to be 7 $\pm$ 1 μm.

Contact angle measurement

To examine the surface wettability (hydrophobicity), the ternary-phase contact angles of sessile liquid samples (3 μL) on the prepared surfaces were measured under room temperature and pressure on a custom-built, vibration-free test bed. Images of the droplets were captured using an AVT Guppy NIR CCD color camera with a 9.8–77 mm video zoom lens (Edmund Optics) and a light diffuser. The captured images were processed by ImageJ with the Dropsnake and LB-ADSA plugins, in which contact angles on the left and right side of each droplet were measured and averaged. Three replicate droplets of each sample were measured.

Image analysis to quantitate the fractional area of toner printed at different gray-scale level

Image of the prepared transparency films were magnified by 20 fold under a microscope (Axio Scope A1, ZEISS) and captured by a camera with CMOS sensor (PL-B681CU, PixeLINK). TIF image files were processed into binary with the gray level threshold set by an isodata algorithm written in Mathematica software. The fractional area of toner was obtained by dividing the number of dark pixels over the total number of pixels.

Fabrication of toner-based valves on PeT microdevices

For the fabrication of PeT microdevices described in the literature to-date,[11,28–31] a dense layer of toner is patterned by a laser printer selectively on the transparency sheets to serve as an adhesive to bond the two layers together. This very same fabrication process is obviously compatible with the step needed to incorporate toner-based valves by precisely patterning toner (at predetermined densities) in select locations in the microchannel. We modified the method described by Duarte *et al.* for PeT chip fabrication,[29] as it yielded microchannel depths functional and comparable to those applications utilized in many microfluidic devices (*e.g.*, glass, PDMS, PMMA) reported for biological assays.[16,46,47] The main fabrication steps are shown schematically in Fig. 2. First, only the underside of the top (L1) and topside of bottom (L3) transparency layers were selectively patterned with toner [3 mm (w) × 2 mm (l) patches] to define the hydrophobic valve, while both sides of middle transparency layer (L2) were uniformly coated by two layers of printer toners (the final thickness of the middle layer after printing was measured to be 132 $\pm$ 3 μm). The L1 and L2 layers were then ablated by a CO_2 laser system according to the design: access holes are cut through L1 as reservoirs and the microchannel out of L2 to define the fluidic network. Following laser ablation, three or four layered devices were created by sandwiching the uniformly toner-coated layer(s) between L1 and L3 layers, visually aligned and inserted into a heated roll laminator with a temperature setting at 130 °C and a speed setting of 2.5 mm s^{-1} (Model 305, Mega Dry film laminator).

It is during this lamination step that the toner coating on L2 bonds the neighbouring polyester layers. The patterned toner patches on L1 and L3 constitute a section the ceiling and floor of the valve region, and since these are air-filled and separated by the thickness of the middle spacing layer(s) (L2), their hydrophobic character is preserved enough to serve as a hydrophobic valve. It is noteworthy that the integration of toner valves on the PeT microdevices adds negligible extra cost ($\sim$ \$ 0.007 for 100 valves), additional fabrication time ($\sim$1 min).

Determine the contact angle on the sidewall

Three and four-layer PeT microdevices with no toner-based hydrophobic valves were fabricated which has a 60 mm long channel. The actual width of the channel after lamination was experimentally measured under microscope. The microdevice was inserted into the DI water vertically with one end of the channel immersed under the water surface. The water wicked into the channel by capillary force until it was balanced by the gravity. Therefore, one can obtain the relationship between the surface property and observed height difference (H_1) between the water column in the channel and water level around the microdevice. The pressure generated by gravity is $\rho g H_1 . \cos\theta_w$ could be solved by plugging the calculated value of $\rho g H_1$ to eqn (2).

Characterization of burst pressure

In the study of burst pressure, we fabricated three and four layers of PeT microdevices which have a 20 mm long channel with a toner valve 2 mm away from the outlet. Experimental burst pressures of the hydrophobic toner valves were obtained by a microflow method described elsewhere.[43] Briefly, the inlet of the channel was connected to a straight pipette. The initial addition of deionized water wetted through the channel until it came to the hydrophobic zone. Deionized water was gradually added into the pipette until the water height (H_2) reached a critical value driving the liquid past the hydrophobic zone. The pressure generated by the water column is $\rho g H_2$, which can be used with eqn (2).

Determining the burst frequency of the valve on a centrifugal system

PeT microdevices with toner valves were placed on a spinning setup comprised of a computer-controlled motor (5 : 1 Micro Metal Gearmotor HP) to precisely modulate rotational frequencies *via* voltage input (0–6 V). Distilled water was loaded through the inlet which automatically priming the channel until the water was stopped by the toner valve. The critical

Table 1 Contact angles for deionized water on the different surfaces. The standard deviation of all measurements is ± 3° (n = 3)

Material	Transparency film	Black (HP)	Black (Brother)	Magenta (Brother)	Cyan (Brother)	Yellow (Brother)
Contact angle	51°	111°	96°	99°	91°	96°

burst frequency was obtained by gradually increasing the rotational speed at intervals of ~30 rpm until water was observed in the receiving chamber.

Results and discussion

Selection of printer toners

The compositions of commercially-available toners differ significantly from brand to brand. For example, according to the MSDS, the black toner in an HP printer is composed of iron oxide (45–55% wt/wt) and a styrene/acrylate copolymer (a ratio of 1 : 4.6, 45–55% wt/wt).[28] In contrast, the black toner in a Brother printer, as recorded in MSDS, generally have a higher weight percentage of styrene-acrylate copolymer (85–87% wt/wt) mixed with fatty acid ester (4–6% wt/wt), pigment (4–6% wt/wt), PMMA (1–3% wt/wt) and silicon dioxide (1–3% wt/wt). We tested the hydrophobicity of both brands of printer toner patterned on polyester at maximum density by measuring the contact angle of deionized water.

As summarized in Table 1, all of the toners increase the contact angle effectively in comparison with untreated transparency film, with the largest increase in contact angle provided by the HP toner. As indicated by eqn (1), a relatively large contact angle from the toner provides a wider range for manipulation of surface hydrophobicity *via* gray-scale level graphic control. As a result, the HP black toner was selected for all the work that follows.

With HP toner patterned at 100% gray-scale level, we probed the contact angle associated with a number of different reagents commonly used in biochemistry protocols of interest to our lab (Table 2). While the HP toner proved to be a reliable and relatively inert hydrophobic coating for most aqueous solutions, its stability in the presence of organic solvents or surfactants was poor (data not shown), consistent with many other reported hydrophobic valves.

Printer toner has been previously been shown to be inert to variety of chemicals.[28] Successful DNA extraction, PCR amplification,[29] protein concentration and purification[11] have been demonstrated on PeT microdevices and suggest that there is a small, if any, effect of these on performance. In addition, considering the contact surface area (<1.6 mm^2) and exposure time to reagents are small, chance that adverse interactions (*e.g.*, absorption) occur is minimized. Furthermore, if there is concern over potential redox effect from contact between encapsulated iron oxide and samples/reagents in certain applications, purely polymeric-based toners (*e.g.*, Brother toner) can be used as an alternative. Admittedly, contamination of the samples by direct contact with the toner surface is always a potential issue but our experience, thus far, has been that this is not problematic with this valving process.

Characterization of the toner-coated surface on PeT

We first needed to validate that the use of gray-scale level control of printing could provide a graded change in the fractional area of the toner-modified surface, which consequently changes the hydrophobicity. This was accomplished by capturing images of the toner surfaces under a light microscope (Fig. 4A) and using image analysis software to quantitate the fractional area covered by toner for correlation with the gray-scale level setting. As shown in Fig. 4B, there is a defined relationship between the fractional area of toner surface and the gray-scale level value.

When the value of the gray-scale level increased from 50% to 70%, the micropattern of the toner surface changed from separated clusters to a honeycomb-like network. We further measured the contact angle of DI water on toner surfaces printed at different gray-scale levels and these results (Fig. 4C) show that the cosine value of the experimentally-determined contact angle decreased linearly as the fractional area of toner surface increased, in agreement with eqn (2). Interestingly, only when the value of gray-scale level was >60% did the toner-modified surface possess adequate hydrophobicity (contact angle >90°), and this correlated with the appearance of the honeycomb network microfeature. Inter-day reproducibility of the contact angle was ± 3° (n = 3). This confirmed that control of the gray-scale level could provide a graded microscale change the surface, and that a gray-scale level value >60% should be used to effectively create a hydrophobic surface that could provide valuing functionality.

Characterization of the laser-ablated sidewall on PeT microdevice

Along with the top and bottom surfaces of the toner valves, the quality of the sidewall is equally important because it also contributes to the reliability and robustness of the burst valves. We used an indirect but simple method to calculate the effective contact angle of DI water on the sidewall, as an assessment of the inter-day reproducibility of the heteroge-

Table 2 Contact angle of different biological relevant reagents on the HP toner coating. The standard deviation of all measurements is ± 3° (n = 3)

Reagent	Distilled Water	TE Buffer	PCR Buffer	6M GuHCl (pH = 7.4)	1% BSA in PBS (pH = 7.4)	HCl (pH = 1)	NaOH (pH = 13)
Contact angle	111°	106°	114°	106°	106°	110°	109°

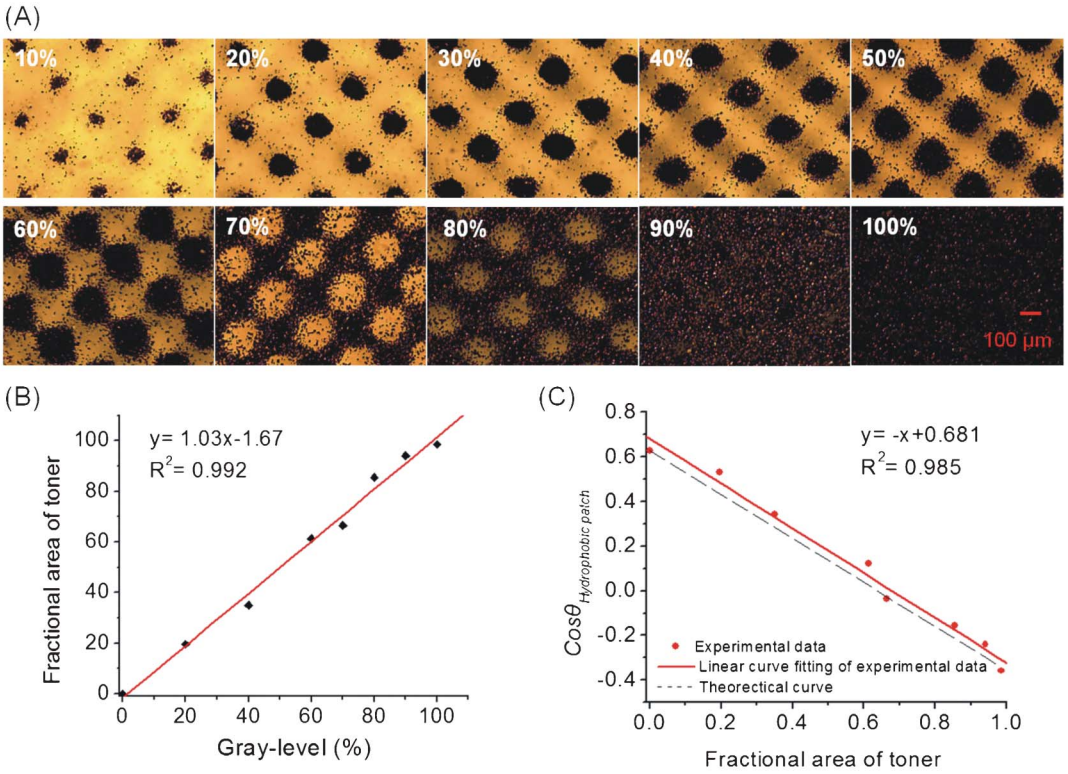

Fig. 4 Characterization of the toner surfaces printed at different gray-scale control. (A) Photographs of the printed hydrophobic toner patches with different gray-levels. (B&C) Plots showing the correlation of the fractional area of toner relative to the value of gray-scale level (B), and the cosine value of the contact angle on the heterogeneous surface relative to fractional area of the toner (C).

neous surface (the basis for using this method was explained in the Theory section.) The effectiveness of the laser ablation of the PeT is dependent on the laser power, the pulse frequency and the laser translation speed, all of which contribute to the change in the effective contact angle of the sidewall (see the ESI). In addition, because of the zone affected by a single laser pulse on transparency film is between ~400 μm in diameter, as the laser 'vects' an edge of the square channel, it affects the mechanical and physical properties of the PeT that will comprise the adjacent wall (within ~200 μm). Thus, the laser ablation of a square channel narrower than 200 μm may lead to somewhat different PeT properties than that of a square channel with a width greater than 300 μm. As a result, the contact angle for a 200 μm wide channel was 103° ± 2°, while those channel widths >300 μm was 126° ± 4° for channels wider than on three-layer PeT microdevices. For one set of fabrication parameters for a channel with defined microfeatures (*i.e.*, width and depth) the inter-day reproducibility of the contact angle is comparable to other hydrophobic valves.[42,43] The effective contact angle of the sidewall in a three- and four-layered PeT microdevices fabricated for our experiments was found to be 126° ± 4° and 98° ± 3°, respectively, for a channel width greater than 300 μm (n = 3). Since these two multilayer devices have respective channel depths of 132 μm or 264 μm, certainly in the range of most common microfluidic devices, we did not investigate the PeT microdevices with more than four layers in this study.

Influence of the channel geometry on burst pressure

Previous studies anchored on eqn (2), have shown that with a given surface property, the burst pressure is dependent on the valve dimensions (width and depth) and has been observed and validated on microchips using many different substrates including PMMA,[44] PDMS[26] and CHF_3 modified glass.[43] Here, the influence of the channel geometry on burst pressure was investigated by varying the width of channels that had a depth of 132 μm with toner patterned on the surface printed at 100% gray-scale level. The channel widths investigated ranged from 250–800 μm; widths narrower than this suffered from occlusion, while larger ones were prone to deformation during thermal lamination. The observed and theoretical burst pressures (from eqn (2)) were plotted against the channel width in Fig. 5A. Limited by the resolution of the laser ablation system (~100 μm) and thermal lamination constraints, the burst pressure change controlled by a simple change in channel width was determined to be 492 (± 18) Pa at 800 μm and 573 (± 16) Pa at 400 μm. There is a break in the trend below 400 μm, and this observation is likely explained by the fact that the contact angle along the sidewall of a 250 μm wide channel is smaller than the contact angle of channels wider than 300 μm, a direct consequence of potentially modifying adjacent PeT during the ablation process (discussed in the previous section). This deviation in trend could arise from: (1) the use of a static contact angle instead of the advancing contact angle, (2) the differences in contact angle on a freshly

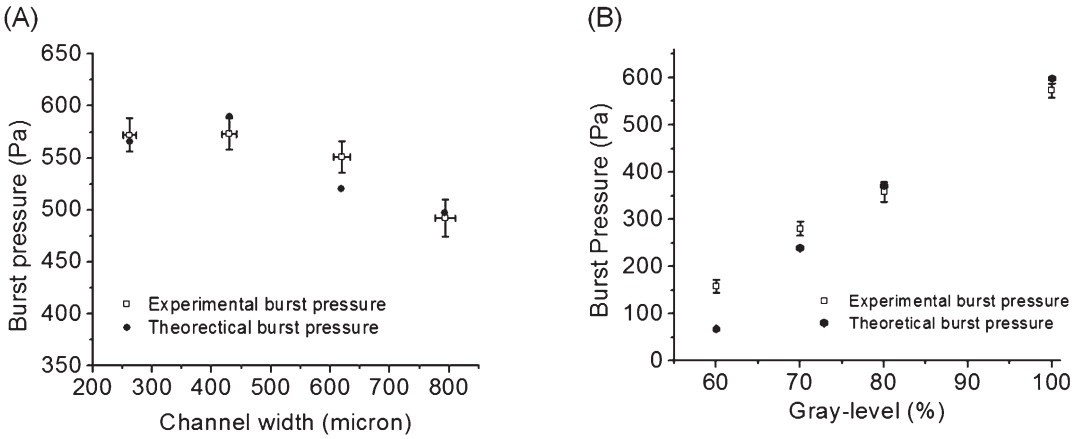

Fig. 5 Characterizing the burst pressure of toner-based valves on PeT microchips. Experimental and theoretical results for valve burst pressure *versus*: (A) the width of the channel with deionized water and (B) the fractional area of HP toner with deionized water. The error bars represent one standard deviation (n = 5).

printed toner surface *versus* toner surface in a channel, where heating during lamination may alter the surface since the temperature is close to the glass transition temperature, and (3) the use of a mean value for the contact angles (*e.g.*, θ_w)

Influence of gray-scale level on burst pressure

The effectiveness of varying the gray-scale level to change the surface hydrophobicity and, thus, control the valve burst pressure was studied by printing microareas of transparency film with toner at different gray-scale levels (>60%) with constant channel geometry [400 μm (w) × 264 μm (d)]. Plots of the experimental and calculated burst pressures [eqn (2)] *versus* the gray-scale level are given in Fig. 5B. There is only a small discrepancy between the two data sets, indicating the successful application of the Cassie model to the toner microarea patterning *via* laser printing lithography. More significantly, the operational band width of burst pressures, from 158 ± 18 Pa to 573 ± 16 Pa, covers a 415 Pa range, a 5-fold improvement over the bandwidth obtainable with geometrical valves (80 Pa). Subsequently, this presents the possibility of tailoring laser-printed toner valves with burst pressures that meet the specification of the pressure sources used for fluid mobilization. One can envision sources that range from the precision of an automated syringe-type pump to a manual 'finger-driven' pump, or centrifugally-driven force from a battery-powered motor (*e.g.*, a motor from a CD drive).

Toner-valve performance in a centrifugal microfluidic chip

For further validation of toner valve performance, PeT microdevices with 100% gray-scale toner valves and different channel dimensions were integrated into a rotating microfluidic system. The calculated and experimental burst frequencies, in rpm, with different valve dimensions on the centrifugal system are given in Table 3.

The experimental results are in reasonable agreement with theoretical predictions given by eqn (5). The difference between the experimental and calculated values, however, can be partially explained by that the pressure calculated by eqn (5) is an equivalent pressure head and can deviate from the actual pressure experience at the toner valve on the centrifugal system and/or a limitation in accurately setting the rotation speed (limitation of the motor and control). Nevertheless, these results validate the functionality of toner valves for centrifugal-microfluidic applications.

Multivalve operation in a centrifugally-driven microfluidic system

Versatile movement and metering of fluids (*i.e.*, sample, buffer reagents) on a centrifugal microfluidic system is essential for biological assays that involve the stepwise addition of reagents.[15,18,20,48] For valves with a given geometry, the burst frequency (in rpm) decreases as the distance from the center of the microchip increases. Therefore, valves with identical geometry positioned in a line radially from the center to the perimeter will, at a particular rotational frequency, have the outer valves burst first. Since centrifugal force drives fluid from the center to the perimeter of the microchip, a valving system that allows for the metering, flow and mixing of reagents loaded at center reservoirs necessitates that valves burst in the proper sequence at increasing rotational speeds.

Table 3 Burst frequency of the toner valves printed at 100% gray-scale level with different dimensional parameters (n = 7)

No.	Channel width/μm	Channel depth/μm	R_1/mm	R_2/mm	Calculated burst frequency/rpm	Observed burst frequency/rpm
1	400	132	20	40	405	353 ± 29
2	400	264	20	40	287	303 ± 22
3	600	132	20	30	628	575 ± 30
4	800	132	20	40	531	480 ± 19

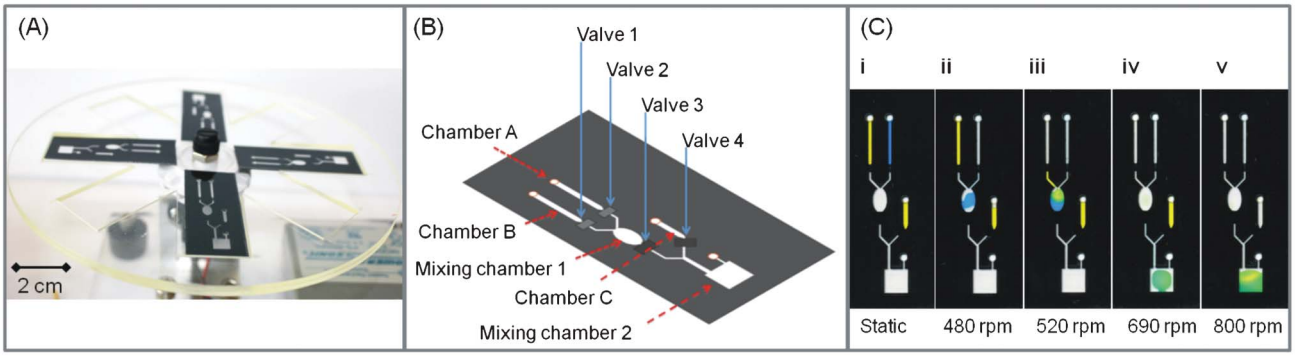

Fig. 6 Demonstrating toner-based hydrophobic valving on centrifugal microchips. (A) Photograph showing PeT microchips containing toner valves on the home-built centrifugal system. (B) Fluidic architecture for sequential valving in the fluidic network. (C) A series of images captured by an office scanner illustrating valving where the steps are: (i) reagent loading, (ii) addition of reagent A (blue dye), (iii) addition of reagent B (yellow dye) to reagent A, (iv) transfer of mixture A&B to downstream chamber, and (v) addition of reagent C (yellow dye).

Knowing that, at a particular rotational speed, the innermost valves must burst first, the channel geometry must decrease from the center outwards. As indicated earlier, geometrical capillary valves provide a relatively narrow operational bandwidth of burst pressures, which will not only limit the number of possible sequential assay steps, but also will increase the risk of valving failure modes. We circumvent this issue by holding geometry constant and using toner valves printed at gray-scale levels of 65% (valve 1), 70% (valve 2) or 100% (valve 3&4) (Fig. 6B). In Fig. 6C, the detail of sequential mixing is illustrated. As shown in Fig. 6B, the microchannel architecture is detailed for three reagents (food dyes) with the toner valves represented by shaded rectangles. Fig. 6C provides a series of images obtained after stepping through four rotational speeds: 480, 520, 690 and 800 rpm. This demonstrates the power of toner valves in geometrically-identical microchannels to have varied burst frequencies based on hydrophobicity.

The direct toner printed valve introduces a new development in fabrication for centrifugally-driven (and other) microfluidic platforms. Programming of sequential reagent delivery on one microdevice can be easily reconfigured by simply alternating the gray-scale level setting for the top and bottom layers while using the same modular design for the middle layer(s), thus relieving the dependency on sophisticated designs of for microfluidic network, as well as demands on the fabrication method(s). Since this reconfigurable feature provides a possible solution for rapid and cost-effective customization of microfluidic devices, it may open the door to more widespread use of PeT as a substrate for advancing LOC technology.

Conclusions

In this work, we have outlined the working principles and fabrication approach to integrate hydrophobic toner valves on PeT microdevices *via* laser printer lithography. Having characterized the relationship between hydrophobicity of a patterned toner surface in the microchannel and the burst pressure, we leveraged the ability to use gray-scale level control to vary the hydrophobicity so that valves require different burst frequencies. The resolution of gray-scale level control in the current (and even older) laser printers is adequate for hydrophobic modification on Pe surface. By printing designs onto transparency film with using toners of different compositions or gray-scale levels, the workable pressure range of burst valves was expanded, and these can be easily integrated to more complex systems to enable sequential delivery of multiple reagents either on pump- or centrifugally-driven microfluidic platforms.

As compared to other commonly used capillary valves, the incorporation of toner-based hydrophobic valves brings convenience to microchip fabrication with several advantages: (1) only one extra printing step is required, (2) highly-precise microstructures for burst pressure control can be eliminated, (3) there is zero additional fabrication time as the number of valves increases, and (4) there is potential for reprogramming an integrated microfluidic network *via* reconfiguration of the print setting for each valve. In addition, this laboratory fabrication protocol may present new potential for industry-scale production used the currently-existing range of roll-based integration technologies for printing and lamination. Details on the manufacturing engineering details for such a device, as well as the putative cost to mass manufacturing are beyond the scope of this paper.

Although we have demonstrated an inexpensive and rapid approach to fabricate microfluidic systems with passive valves allowing for a four-step reagent delivery, we acknowledge that several issues need to be addressed before this approach could be used as a cost-effective, disposable cartridge for the point-of-care analysis in the resource-limited-situations. For example, the hydrophobic toner patches do not provide a vapour barrier, therefore, on-chip storage of the liquid reagents could be problematic. This could be addressed using dried/lyophilized reagents which can be reconstituted when buffer or sample is loaded; such feasibility has been demonstrated by Focke *et al.*[8] on polymeric-based microchips (although using a non-PeT substrate). For some assays that may require a high

centrifugal speed as the first step (*e.g.*, ~3600 rpm to separate plasma from the red blood cells[1]), toner valves will be insufficient. However, due to the hydrophilic property of the commercial Pe film, a siphoning structure similar to those shown by Ducrée's group[49,50] could be adopted. Additionally, the burst pressure bandwidth of the toner valves is not as broad as phase-change valves,[37–39] thus it is challenging to achieve eight or nine sequential reagent addition steps at this point. However, we are evaluating a number of approaches to enhance the burst pressure bandwidth. Future work will focus on the use of toner-based valves to achieve automated, paralleled, comprehensive biological assays on a portable centrifugally-driven PeT microdevice platform.

References

1 J. Park, V. Sunkara, T.-H. Kim, H. Hwang and Y.-K. Cho, *Anal. Chem.*, 2012, **84**, 2133–40.
2 B. S. Lee, Y. U. Lee, H.-S. Kim, T.-H. Kim, J. Park, J.-G. Lee, J. Kim, H. Kim, W. G. Lee and Y.-K. Cho, *Lab Chip*, 2011, **11**, 70–8.
3 S. Lai, S. Wang, J. Luo, L. J. Lee, S.-T. Yang and M. J. Madou, *Anal. Chem.*, 2004, **76**, 1832–7.
4 D. C. Duffy, H. L. Gillis, J. Lin, N. F. Sheppard and G. J. Kellogg, *Anal. Chem*, 1999, **71**, 4669–4678.
5 M. Grumann, J. Steigert, L. Riegger, I. Moser, B. Enderle, K. Riebeseel, G. Urban, R. Zengerle and J. Ducrée, *Biomed. Microdevices*, 2006, **8**, 209–14.
6 S. J. Vella, P. Beattie, R. Cademartiri, A. Laromaine, A. W. Martinez, S. T. Phillips, K. A. Mirica and G. M. Whitesides, *Anal. Chem.*, 2012, **84**, 2883–91.
7 Y. Zhang and P. Ozdemir, *Anal. Chim. Acta*, 2009, **638**, 115–25.
8 M. Focke, F. Stumpf, B. Faltin, P. Reith, D. Bamarni, S. Wadle, C. Müller, H. Reinecke, J. Schrenzel, P. Francois, D. Mark, G. Roth, R. Zengerle and F. von Stetten, *Lab Chip*, 2010, **10**, 2519–26.
9 E. T. Lagally, C. A. Emrich and R. A. Mathies, *Lab Chip*, 2001, **1**, 102–7.
10 M. J. Heller, *Annu. Rev. Biomed. Eng.*, 2002, **4**, 129–53.
11 H. Yu, Y. Lu, Y. Zhou, F. Wang, F. He and X. Xia, *Lab Chip*, 2008, **8**, 1496–501.
12 Z. Zhu, J. J. Lu and S. Liu, *Anal. Chim. Acta*, 2012, **709**, 21–31.
13 J. Gao, X.-F. Yin and Z.-L. Fang, *Lab Chip*, 2004, **4**, 47–52.
14 S. Lindström and H. Andersson-Svahn, *Lab Chip*, 2010, **10**, 3363–72.
15 J. Ducrée, S. Haeberle, S. Lutz, S. Pausch, F. Von Stetten and R. Zengerle, *J. Micromech. Microeng.*, 2007, **17**, S103–S115.
16 C. J. Easley, J. M. Karlinsey, J. M. Bienvenue, L. A. Legendre, M. G. Roper, S. H. Feldman, M. A. Hughes, E. L. Hewlett, T. J. Merkel, J. P. Ferrance and J. P. Landers, *Proc. Natl. Acad. Sci. U. S. A.*, 2006, **103**, 19272–7.
17 K. W. Oh and C. H. Ahn, *J. Micromech. Microeng.*, 2006, **16**, R13–R39.
18 M. Madou, J. Zoval, G. Jia, H. Kido, J. Kim and N. Kim, *Annu. Rev. Biomed. Eng.*, 2006, **8**, 601–28.
19 C. D. Chin, V. Linder and S. K. Sia, *Lab Chip*, 2007, **7**, 41–57.
20 R. Gorkin, J. Park, J. Siegrist, M. Amasia, B. S. Lee, J.-M. Park, J. Kim, H. Kim, M. Madou and Y.-K. Cho, *Lab Chip*, 2010, **10**, 1758–1773.
21 F. Reymond and P. E. Michel, *Polymer*, 2002, 858–867.
22 C.-W. Tsao and D. L. DeVoe, *Microfluid. Nanofluid.*, 2008, **6**, 1–16.
23 D. C. Duffy, J. C. McDonald, O. J. Schueller and G. M. Whitesides, *Anal. Chem.*, 1998, **70**, 4974–84.
24 M. Hitzbleck, L. Avrain, V. Smekens, R. D. Lovchik, P. Mertens and E. Delamarche, *Lab Chip*, 2012, **12**, 1972–8.
25 B. Mosadegh, H. Tavana, S. C. Lesher-Perez and S. Takayama, *Lab Chip*, 2011, **11**, 738–42.
26 H. Cho, H.-Y. Kim, J. Y. Kang and T. S. Kim, *J. Colloid Interface Sci.*, 2007, **306**, 379–85.
27 W. K. T. Coltro, S. M. Lunte and E. Carrilho, *Electrophoresis*, 2008, **29**, 4928–37.
28 C. L. do Lago, H. D. T. da Silva, C. A. Neves, J. G. A. Brito-Neto and J. A. F. da Silva, *Anal. Chem.*, 2003, **75**, 3853–8.
29 G. R. M. Duarte, C. W. Price, B. H. Augustine, E. Carrilho and J. P. Landers, *Anal. Chem*, 2011, **83**, 5182–5189.
30 A.-L. Liu, F. He, K. Wang, T. Zhou, Y. Lu and X. Xia, *Lab Chip*, 2005, **5**, 974–8.
31 A.-L. Liu, T. Zhou, F.-Y. He, J.-J. Xu, Y. Lu, H.-Y. Chen and X.-H. Xia, *Lab Chip*, 2006, **6**, 811–8.
32 M. A. Roberts, J. S. Rossier, P. Bercier and H. Girault, *Anal. Chem.*, 1997, **69**, 2035–42.
33 Y. Liu, H. Lu, W. Zhong, P. Song, J. Kong, P. Yang, H. H. Girault and B. Liu, *Anal. Chem.*, 2006, **78**, 801–8.
34 J. S. Rossier and H. H. Girault, *Lab Chip*, 2001, **1**, 153–7.
35 J. Ji, Y. Zhang, X. Zhou, J. Kong, Y. Tang and B. Liu, *Anal. Chem.*, 2008, **80**, 2457–63.
36 J. L. Garcia-Cordero, D. Kurzbuch, F. Benito-Lopez, D. Diamond, L. P. Lee and A. J. Ricco, *Lab Chip*, 2010, **10**, 2680–2687.
37 D. J. Beebe, J. S. Moore, J. M. Bauer, Q. Yu, R. H. Liu, C. Devadoss and B. Jo, *Nature*, 2000, **404**, 588–590.
38 K. Abi-Samra, R. Hanson, M. Madou and R. Gorkin, *Lab Chip*, 2011, **11**, 723–6.
39 R. Gorkin, C. E. Nwankire, J. Gaughran, X. Zhang, G. G. Donohoe, M. Rook, R. O'Kennedy and J. Ducrée, *Lab Chip*, 2012, **12**, 2894–902.
40 R. L. Hoffman, *J. Colloid Interface Sci.*, 1975, **50**, 228–241.
41 L. Gao and T. J. McCarthy, *Langmuir*, 2006, **22**, 6234–7.
42 H. Andersson, W. Van Der Wijngaart, P. Griss, F. Niklaus and G. Stemme, *Sens. Actuators, B: Chemical*, 2001, **75**, 136.
43 Y. Feng, Z. Zhou, X. Ye and J. Xiong, *Sens. Actuators, A*, 2003, **108**, 138–143.
44 C. Lu, Y. Xie, Y. Yang, M. M.-C. Cheng, C.-G. Koh, Y. Bai, L. J. Lee and Y.-J. Juang, *Anal. Chem.*, 2007, **79**, 994–1001.
45 M. J. Madou, L. J. Lee, S. Daunert, S. Lai and C. Shih, 2001, 245–254.
46 N. J. Cira, J. Y. Ho, M. E. Dueck and D. B. Weibel, *Lab Chip*, 2012, **12**, 1052–9.
47 J. Lounsbury, B. L. Poe, M. Do and J. P. Landers, *J. Micromech. Microeng.*, 2012, **22**, 085006.
48 N. Godino, R. Gorkin III, A. V. Linares, R. Burger and J. Ducrée, *Lab Chip*, 2013, **13**, 685–694.
49 S. Haeberle, T. Brenner, R. Zengerle and J. Ducrée, *Lab Chip*, 2006, **6**, 776–781.
50 J. Steigert, T. Brenner, M. Grumann, L. Riegger, S. Lutz, R. Zengerle and J. Ducrée, *Biomed. Microdevices*, 2007, **9**, 675–9.